



# The feasibility of CO<sub>2</sub>-laser-induced breakdown spectroscopy for fast lead determination in glass cullet

Sebastian Lehmann | Maike Fischer | Andreas Rosin | Thorsten Gerdes |  
Walter Krenkel

Keylab Glass Technology, Department of Ceramic Materials Engineering, University of Bayreuth, Bayreuth, Germany

## Correspondence

Sebastian Lehmann, Keylab Glass Technology, Department of Ceramic Materials Engineering, University of Bayreuth, 95447 Bayreuth, Germany.  
Email: sebastian.lehmann@uni-bayreuth.de

## Funding information

European Regional Development Fund, Grant/Award Number: 20-3066-03-16

## Abstract

With an overall collection and recycling rate of 74%, the material cycle for glass packaging is well established in the European Union. However, knowledge of the composition of the recycled glass cullet is necessary to avoid creeping accumulation of undesirable contaminants into the material cycle. Due to their toxic properties, this applies in particular for heavy metals, for example, lead. The state-of-the-art technology for detection of lead in recycling glass sorting is X-ray fluorescence (XRF). Due to lower regulatory demands, as well as increasingly economical hardware, laser-based detection techniques, like Laser-Induced Breakdown Spectroscopy (LIBS) may provide an alternate approach in industrial glass sorting to reach comparable detection limits and rates. In our work, CO<sub>2</sub>-LIBS was investigated as an alternative tool for the determination of lead in glass cullet. Instead of usually utilized spectrometers, a combination of spectral filters and photodiode was employed to facilitate a fast detection rate. Glass samples with different lead content were investigated in two spectral ranges with respect to detection limits, detection speed, and accuracy. The results are compared to a commercial XRF-sorting machine for glass cullet. It was found that comparable speeds and accuracies for lead detection in glasses can be reached.

## KEYWORDS

LIBS, measurement, properties, quality control, raw materials

## 1 | INTRODUCTION

The material cycle for glass packaging is well established in the European Union, proofing that an almost closed-loop-economy is possible for the valuable raw material glass.<sup>1</sup> Besides the conservation of natural resources, the integration of recycled glass cullet into container glass production decreases the energy demand for melting and

reduces CO<sub>2</sub>-emission.<sup>2–4</sup> However, to ensure a continuous high quality of the glass packaging products, an accurate knowledge of the composition of the recycled glass cullet is necessary. Otherwise, there is the risk of a long-term creeping accumulation of undesirable contaminants, in particular heavy metals. Such unwanted contaminants most likely enter the glass material cycle accidentally, for example, by wrong throws in container glass collection

This is an open access article under the terms of the Creative Commons Attribution License, which permits use, distribution and reproduction in any medium, provided the original work is properly cited.

© 2019 The Authors. International Journal of Applied Glass Science published by American Ceramics Society (ACERS) and Wiley Periodicals, Inc.

system. Additionally, certain metals and metal oxides, like chromium, cobalt or copper as well as arsenic oxide, were or are still used, for example, as coloring and finishing agents. Particularly lead oxide is known for a lowering of the melting temperature and providing a glass with increased density, refractive index, and brilliance, respectively.<sup>5</sup> Intensified by the worldwide decline of usage of lead glass products, especially in the field of CRT-monitors, and insufficient collection and recycling strategies, the accumulation of lead in container glass is a challenge to be encountered. Even if migration of lead from glasses in food-contact applications is generally considered very low, a long-term accumulation as well as the release of heavy metals during the manufacturing process of recycled glass cullet may still bear risks for the human body.<sup>6–9</sup> Hence, several efforts have been made to regulate content and migration of lead and other heavy metals in and from glass and ceramics, for example, an upper limit for heavy metal concentration (Pb, Cd, Hg, Cr<sup>6+</sup>) of 250 ppm in glass packaging.<sup>10,11</sup> In future, legal thresholds might become even stricter.<sup>12,13</sup>

To prevent heavy metal accumulation in recycled glass, a high effort is put in detection and sorting of glass cullet, especially in the container glass industry.<sup>14</sup> Moreover, lead in particular is a valuable second raw material, leading to the development of several techniques for its extraction from glass during the last years, eg by hydrothermal or pyrometallurgical treatment.<sup>15,16</sup> Extraction rates above 90% could be achieved, though investigations were performed mainly on laboratory scale.<sup>17</sup>

A state-of-the-art technology for the detection of lead glass is X-ray fluorescence (XRF). In XRF, atoms are excited by X-ray radiation. During relaxation, characteristic fluorescence light is emitted, which can be detected and utilized for material identification.<sup>18</sup> It can serve as a highly precise and reliable detection tool for example, in forensic science, but can also be employed in industrial scale sorting machines.<sup>19,20</sup> In the latter case, throughput rates typically reach up to 28 tons per hour, and the sortable size ranges lie between 3 and 60 mm. The detection limits are reported in the low percent range.<sup>21</sup> However, regulatory restrictions on use of X-ray equipment are high. Further, there is still a risk of incorrect sorting, especially for smaller cullet and low lead contents. Here, laser-based detection techniques, like laser-induced breakdown spectroscopy (LIBS), may provide a supplemental or even alternate approach. Not only that laser systems can match minimal regulatory demands, they also become more and more economic.<sup>22,23</sup> Further, comparable detection limits and rates can be reached.<sup>24</sup>

In our work, LIBS was investigated as an alternative tool for the determination of lead in glass cullet. In the recent years, LIBS has proven to be a versatile tool for a rather

simple, fast and qualitative as well as quantitative analysis of different samples under different conditions.<sup>25–29</sup> The technique covers also a wide scope in industrial application, for example, in different sorting processes of scrap metals.<sup>23,30</sup> The LIBS working principle is based on plasma generation by focusing laser radiation on a surface. The emitted light from the plasma is analyzed, for example, by spectroscopic means, and information about sample composition is derived. The LIBS technique is described in more detail elsewhere<sup>31,32</sup> and sources within.

In this paper, a pulsed CO<sub>2</sub>-laser with high pulse repetition rate was used to generate plasma plumes on glass. Besides a usually utilized spectrometer, which is useful for a spectrally highly resolved investigation of the generated plasma, a combination of spectral filters and photodiode was employed to achieve a fast detection rate. Glass samples with different amounts of lead were investigated in two spectral ranges for different pulse frequencies with respect to detection limits, detection speed, and accuracy. The results are compared to a commercial XRF-sorting machine for glass cullet.

## 2 | EXPERIMENTAL PROCEDURE

### 2.1 | Sample preparation and characterization

In order to show the feasibility of CO<sub>2</sub>-LIBS for lead detection in glass sorting over a wide range of lead contents, five sample glass discs with different chemical composition were prepared in advance. Each has a diameter of 3.5 cm and a height of approximately 1 cm. Before probing, their composition was investigated by X-ray fluorescence analysis (ZSX Primus II, Rigaku Europe SE, Neu-Isenburg, Germany). The results are shown in Table 1. Typical lead percentages between 1 and 25 wt% were obtained by melting different fractions of a colorless lead-free flint glass and a colorless tableware lead glass, which justifies the variations in the other elements.

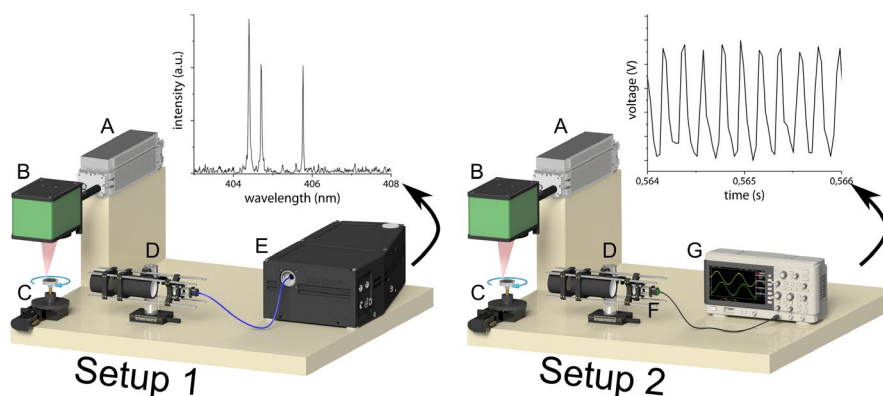
### 2.2 | Experimental setup

Figure 1 schematically shows the experimental LIBS setup. The pulses of a waveguide CO<sub>2</sub>-laser (DEOS LC-100NV, DeMaria ElectroOptics Systems, Inc) with pulse width range >1 μs, repetition rates 1–25 kHz and wavelength of 10,6 μm, operated in gated CW-mode, were guided on the sample surface by a 2-axis deflection unit (RLA-1504, Raylase AG) with a focal length of 30 cm. The laser power is controlled by combining different pulse lengths and repetition rates, for example, a pulse length of 50 μs and

**TABLE 1** Chemical composition of the investigated glass samples, determined by X-ray fluorescence (ZSX Primus II, Rigaku Europe SE, Neu-Isenburg, Germany)

/wt%	Sample 1	Sample 2	Sample 3	Sample 4	Sample 5
SiO <sub>2</sub>	72.8	70.9	68.5	66.1	61.8
Al <sub>2</sub> O <sub>3</sub>	1.0	0.9	0.7	0.5	0.1
K <sub>2</sub> O	0.9	2.1	3.6	5.1	7.8
Na <sub>2</sub> O	12.6	11.2	9.5	7.8	4.7
PbO	1.0	5.0	10.0	15.0	24.0
Sb <sub>2</sub> O <sub>3</sub>	—	—	—	—	0.3
BaO	0.2	0.3	0.3	0.4	0.5
CaO	10.0	8.3	6.2	4.1	0.4
ZnO	—	—	—	—	0.4
MgO	1.2	1.0	0.7	0.5	0.0
Sum	99.7	99.7	99.5	99.5	100,0

Note: The average error of element determination is  $\pm 0.1$  wt%. Deviations from the sum 100 wt% are due to rounding errors and errors in trace element determination.



**FIGURE 1** Schematic representation of the LIBS Setup (A: CO<sub>2</sub>-Laser, B: 2-axis deflection unit, C: sample holder, D: collection optics). In Setup 1 optical emission spectroscopy is conducted with an Echelle spectrometer (E). The Echelle spectrometer is replaced in Setup 2 by lead line specific filters and a fast photodiode (F) connected to a digital oscilloscope (G)

repetition rate of 1 kHz corresponds to 5% of the maximum output of 100 W.

In setup 1, optical emission from the plasma was collected by employing a 90°-setup with the optical axis slightly above and parallel to the sample surface. To identify employable spectral ranges for lead detection, the emission is coupled into a UV glass fiber connected to an Echelle spectrometer (EsaWin4000, LLA Instruments GmbH). The spectral acquisition is triggered by the driving signal of the CO<sub>2</sub> laser to allow a constant gate delay with respect to the laser pulses. The strong emission of the sodium D-line is suppressed by a short pass filter (cut-off wavelength 550 nm), thus limiting the observable spectral range from 300 to 550 nm.

In setup 2, a photodiode for the visible spectral range (BPW21, Siemens, 350-850 nm) connected to a digital oscilloscope (DSOX1102A, Keysight Technologies, Inc) and lead line-specific band pass filters replace the glass fiber for a fast acquisition of data. Filter ranges were 360-370 nm (BP

365 × 10 nm OD4 25 mm, Edmund Optics, Inc) and 400-410 nm (BP 405 × 10 nm OD4 25 mm, Edmund Optics, Inc). Thus, the captured signals represent the plasma emission over the whole lifetime of the plasma, narrowed to the spectral transmission range of the employed filter in each case.

Experiments were conducted with CO<sub>2</sub> laser powers between 5 and 30 W. The pulse width, pulse repetition rates and number of pulses were varied between 20 and 100 μs, between 1 and 6 kHz as well as between 1000 and 6000 pulses, respectively. In each measurement, the center of the sample was placed perpendicular to the laser beam on a height adjustable and rotatable holder in beam focus. Thus, small differences in sample height could be compensated. By rotating the sample (max. 16°/s) and deflecting the laser out of the center (max. 2 mm), a circular ablation area was created. Thus, a too deep penetration of subsequent laser pulses into the sample, resulting in a loss of signal, was prevented. Figure 2 shows Laser Scanning

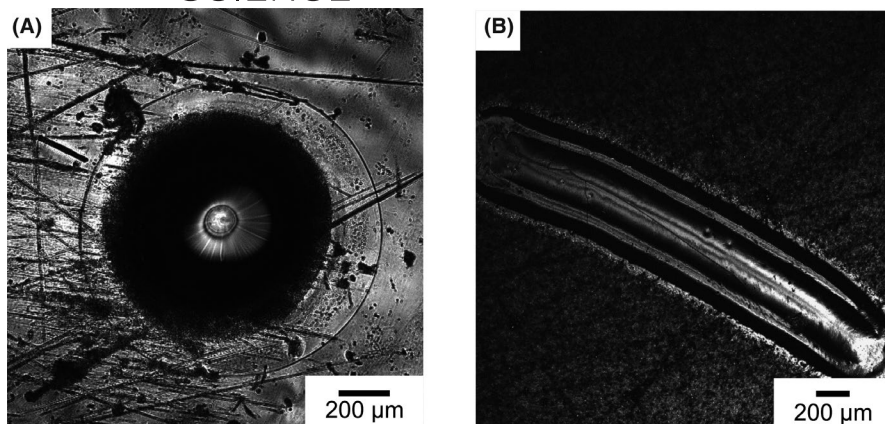


**FIGURE 2** Effect of rotating the sample: After 1000 pulses on the same spot, a crater with depth up to 500  $\mu\text{m}$  is created, leading to loss of signal (A), while for the same conditions on the rotating sample, an arc with a depth of only approx. 80  $\mu\text{m}$  is generated (B). A Laser Scanning Microscope LSM-510 (488 nm, Zeiss, Germany) was employed to obtain both images and depths

Microscopy images (LSM-150, 488 nm) to compare penetration patterns and depths for rotating and nonrotating samples.

### 3 | RESULTS AND DISCUSSION

#### 3.1 | Plasma generation

Due to the dependence of laser power from pulse repetition rate and pulse length, the usable laser power was limited to a quarter of maximum output power. This is based on signal overlap in setup 2, which is discussed in more detail below. Higher laser powers further raise the risk of sample destruction, owned to the induced thermal shock resulting from the high absorption rate in glass at the laser wavelength of 10.6  $\mu\text{m}$ .

Microscopic analysis of generated laser marks shows a focal spot diameter of the  $\text{CO}_2$  laser of about 50  $\mu\text{m}$ . Thus, a power density of at least 0.13  $\text{MW}/\text{cm}^2$  is achieved on the sample surface while the applied laser power was 5 W. The power density was sufficient for material ablation and breakdown, indicated by a bright plasma plume above the sample surface.

#### 3.2 | Optical emission spectroscopy (setup 1)

Prior to the application of the photo diode, plasma emission of the glass samples was investigated by the Echelle spectrometer

in order to identify the relevant spectral ranges for detection of lead-specific emission lines. Spectral data was gathered for all samples shown in Table 1 according to the experimental conditions described above. Up to 40 spectra were accumulated on chip to guarantee an adequate signal intensity. As the detection rate of the Echelle spectrometer is limited to  $f_{\text{Echelle}} = 20$  Hz, an in-house designed trigger unit was employed to record the plasma emission for pulse fractions of  $f_{\text{CO}_2\text{-laser}}/f_{\text{Echelle}}$ . Further, a gate delay of 10  $\mu\text{s}$  after each trigger laser pulse and a gate width of 60  $\mu\text{s}$  were established.

Spectral emission lines were assigned to chemical elements with aid of the NIST database.<sup>33</sup> For all samples, the emission lines of lead at 363.96, 368.35, and 405.78 nm could be identified. Thus, two possible detection ranges were selected. Both are exemplarily demonstrated in Figure 3 for sample 5. They determine on commercially available band pass filters (see below). Range 1 covers wavelengths between 360 and 370 nm. Besides the two emission lines of lead at 363.96 and 368.35 nm, no other emission line and only a weak background signal were monitored. Range 2, encompassing 400–410 nm, contains the emission line of lead at 405.78 nm, which can be monitored easily even for low lead contents. However, due to the rather low plasma temperature, two strong emission lines of potassium (K I 404.41 and K I 404.72 nm) appear in this range.

To consider this in the later time-resolved analysis with photodiode (setup 2), we determined correction factors for the potassium signal in spectral range 2 based on the average

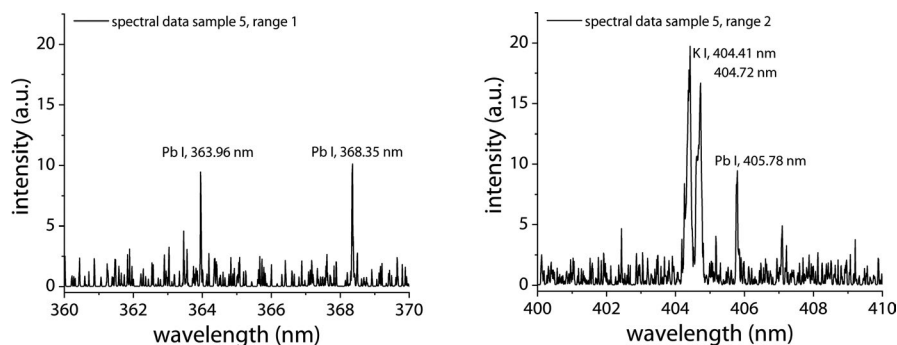


**FIGURE 3** Identification of possible spectral detection ranges for lead emission lines with Echelle spectrometer

potassium signal with respect to the total signal intensity. Peak areas of the potassium signals were determined by integration in five spectra each for sample 2 to 5. Merely for sample 1, lead emission was too weak to be monitored without overexposing the scope of K-lines. By this rather simple approach correction factors for the time-resolved signals in setup 2 could be estimated for samples 2 to 5.

### 3.3 | Optical emission spectroscopy (setup 2)

After specifying the ranges of detection and correction factors, the slow Echelle spectrometer, in terms of laser pulse repetition rate, was replaced by the photodiode and the band pass filters. To identify suitable measuring conditions, plasma emission above each sample's surface was recorded for different pulse powers by varying combinations of pulse repetition rate and pulse lengths in the ranges specified above. Corresponding voltage signals over time were registered with the connected oscilloscope (compare Figure 2). The length of each pulse approximately equates the lifetime of the corresponding plasma, which is between 180 and 200  $\mu\text{s}$  for all measured combinations. For further analysis, spectral emission intensity was identified with the background-corrected area beneath each voltage signal. Following Haddad et al, different figures of merit, specifically the precision and repeatability of the setup, the limit of detection, as well as trueness for concentration determination and rate of correct classification have been investigated to describe the performance of the  $\text{CO}_2$ -LIBS photodiode setup.<sup>34</sup>

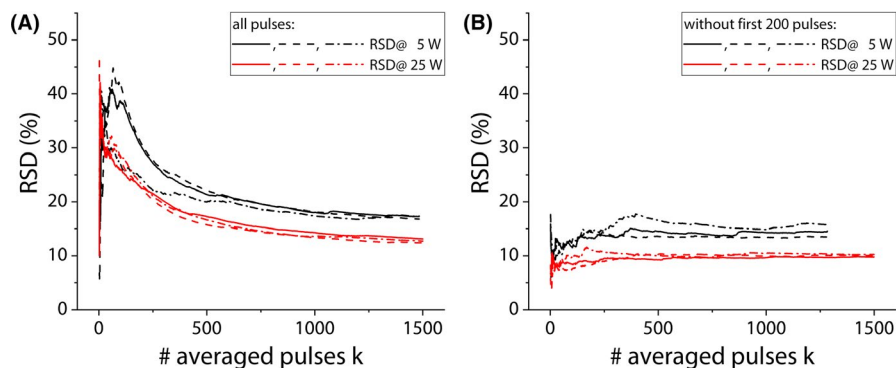
First, the repeatability of the setup was evaluated for two output powers. For the corresponding laser parameters up to 3000 pulses were recorded and for each set of parameters, three measurements were taken. To determine the pulse-to-pulse variation in each measurement series, the mean pulse area and the corresponding relative standard deviation (RSD) were calculated for each series. Additionally, the series-to-series variation was determined. The results are shown in Table 2.

For both series of three with different laser output powers, a good repeatability with low RSD values is achieved, wherein the series with higher output power shows lesser variation. However, within each measurement series rather high RSD values arise for both output powers. Figure 4 shows the RSD of the background-corrected areas under the measured voltage signals as a function of the number of averaged laser pulses,  $k$ , for the different laser powers. While in Figure 4A, all pulses are processed for the two output powers and three measurement series each in Figure 4B the first 200 pulses of the same datasets were excluded from averaging. Utilizing all pulses, much higher RSD values are obtained compared to the second case. This is related to the fact that for each measurement, the laser was run with a defined number of pulses and thereafter stopped either for sample or parameter change. Therefore, the first 200 pulses and their voltage signals, respectively, are subject to start-up deviations of laser power. Hence, they are excluded from further analysis. This measure is appropriate because in later application stages it can be assumed, that no or at least suitable start-up behavior of the laser with constant parameters between single measurements can be assumed. After this first optimization step, slightly lower RSD values of the measured signals, approximately

**TABLE 2** Mean and relative standard deviation (RSD) of pulse areas for each series and overall mean and RSD for all three series for two different laser output powers and up to 3000 pulses

Power/(W)	Series 1		Series 2		Series 3		Series 1 to 3	
	Mean pulse area/ ( $\mu\text{V}$ )	RSD pulse area/ (%)	Mean pulse area/ ( $\mu\text{V}$ )	RSD pulse area/ (%)	Mean pulse area/ ( $\mu\text{V}$ )	RSD pulse area/ (%)	Mean pulse area/ ( $\mu\text{V}$ )	RSD pulse area/ (%)
5	23.7	17.4	24.0	16.8	21.5	17.3	23.1	4.8
25	91.7	11.6	90.0	11.2	87.6	11.4	89.8	1.9

**FIGURE 4** Progress of relative standard deviation (RSD) for different laser powers over different numbers of averaged laser pulses respectively plasma signals  $k$  for spectral range 2 when all (A) or all but the first 200 pulses (B) are considered for averaging



10%-15%, are obtained for different laser powers. Such RSD values are comparable to other LIBS experiments, and are among others the result of natural variations in plasma intensity.<sup>32</sup> Further, less fluctuation is observed between different measurements at 5 and 25 W, again demonstrating a good repeatability. Interestingly, in Figure 4B, RSD values tend to be lower for smaller numbers of averaged pulses,  $k$ , than for the whole range of voltage pulses. This fact is explained by a higher similarity of adjacent plasmas and can be exploited for measurement time reduction, as described below in more detail.

To demonstrate the truth of concentration determination, facile calibration curves were determined for the known lead contents of the investigated glass samples. Though more sophisticated methods exist for determination of concentration, for example, calibration-free LIBS or multivariate analysis, these techniques often require high experimental and numerical efforts.<sup>35</sup> However, this is contrary to the objective of this work to show the feasibility of CO<sub>2</sub>-LIBS as a simple, fast, and economic detection technique for lead in glass cullet.

Plasma emission from 1000 subsequent laser pulses was recorded for a pulse length of 50  $\mu$ s and different pulse repetition rates within the specified spectral ranges for the prepared samples (Table 1). For each sample, five measurements were conducted. Again, the areas beneath voltage signals were determined as a measure for intensity and thus concentration. Data recording was started a few milliseconds prior to activation of the laser. Thus, background and noise of the setup without plasma emission intensity could be determined for each measurement. Compared to the standard deviation of the oscilloscope noise signal, signal-noise-ratios greater than 10 were obtained for all measurements.

As discussed above, the first 200 pulses were omitted. Further, the previously determined correction factors were applied for the second spectral range (400 to 410 nm) to subtract out the amount of the potassium emission line intensities. As

shown previously, RSD values of averaged pulses tend to be lower for smaller number of averaged pulses,  $k$ , than for the whole range of voltage pulses. Therefore, by implementing a moving average function, intensities were determined for different numbers of averaged laser pulses,  $k$ , for all remaining signals and plotted against the previously determined lead content (compare Table 1). As a broad range of lead content is considered in this work, the linearity of the calibration curves may be limited, especially for the samples with higher concentrations of the element.<sup>24</sup> Thus, not only linear but also quadratic calibration functions are supposed for each of these plots. (Figure 5). It was found that in range 1 linear functions are sufficient only for lead contents below 15 wt%. Considering the whole range of lead content, a polynomial fit with order 2 reproduces the measured data appropriately. Figure 5A illustrates the result for those values averaged over all but the first 200 plasma signals. On the contrary, in spectral region 2 a linear function seems sufficient for fitting the data points as shown in Figure 5B. A possible reason for this different behavior might be the reduced lead content range in spectral region 2. As stated above, a corrected intensity signal for sample 1 could not be determined.

By averaging over different numbers of subsequent plasma signals, it was found that reproducible quadratic calibration functions were accessible not only for the full number of pulses. Even five voltage signals were sufficient to generate reproducible calibration parameters. This is exemplarily illustrated in Figure 6. The constant fit parameters  $a_2$ ,  $a_1$ , and  $a_0$  of the quadratic function,

The parameters  $m$  and  $t$  of the linear fit function,

$$y = mx + t,$$

as well as the correlation coefficients  $R^2$  of the calibration function fits are depicted as boxplots for different number of averaged signals  $k$  in both spectral ranges and for pulse

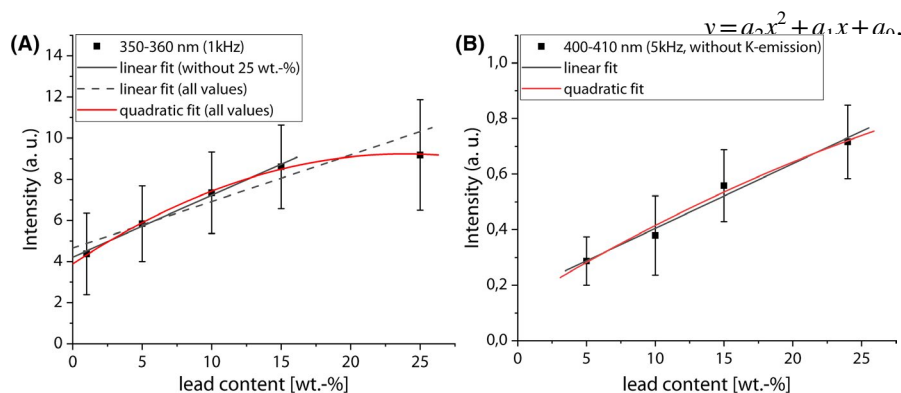


**FIGURE 5** Comparison of linear and quadratic fits for the determination of the calibration function in both spectral ranges. For 360-370 nm (subfigure A), the solid line represents a linear fit over the first four lead contents, the dashed line depicts a line fit over all lead contents. Fitting over the whole range of lead content requires a polynomial order of 2 (solid red). However, for the accessible data in range 2 (400-410 nm, subfigure B), a linear fit seems sufficient

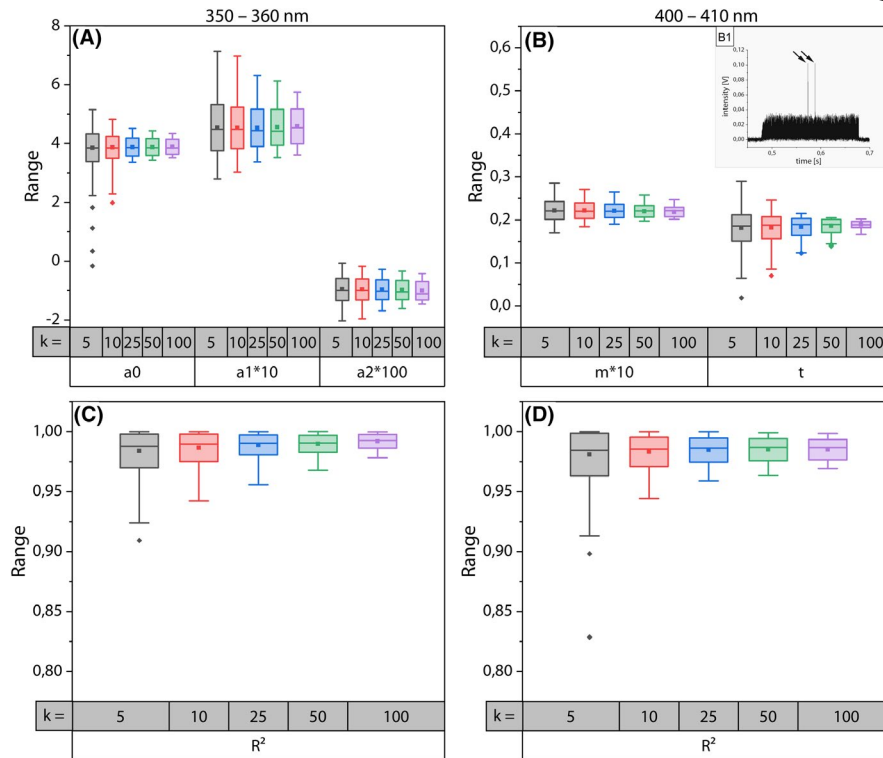


**FIGURE 6** Boxplots of the fitting parameters  $a_2$ ,  $a_1$  (scaled for better visibility) and  $a_0$  for range 1 (360–370 nm),  $m$  (scaled for better visibility) and  $t$  for range 2 (400–410 nm), as well as the correlation coefficients  $R^2$  of the calibration function fits for different number of averaged signals  $k$ . Subfigures A and C show results for a pulse repetition rate of 1 kHz and laser power of 5 W; subfigures B and D represent pulse repetition rates of 5 kHz and laser power of 25 W. The label “Range” represents the values of each plotted variable. Within the boxes, ■ is the mean and— the median. Each box represents the standard deviation of the values, the whiskers indicate the lowest respectively highest datum still within three times the standard deviation. Despite of some outliers due to occasional very high signal peaks (compare inset B1 in the upper right graph B), the fits show a good reproducibility, even for low numbers of averaged signals  $k$

frequencies of 1 kHz (Figure 6A,C) and 5 kHz (Figure 6B,D). For improved visualization,  $a_2$  is multiplied by 100, while  $a_1$  and  $m$  are multiplied by a factor of 10. The label “Range” represents the values of each variable. Within the boxes, each filled square displays the mean, and each line marks the median value. The box represents the standard deviation, while the whiskers indicate the lowest respectively highest datum still within three times the standard deviation.

For all numbers of averaged signals, the mean and the median of the fitting parameters are almost equal, indicating similar fits and thus good reproducibility. In addition, the standard deviation, depicted by box size, only varies slightly. For decreasing numbers of averaged signals  $k$ , the number of outliers and extreme outliers rises. At low pulse repetition rate, they are the result of natural variations of the plasma emission signal, for example, caused by surface ablation artifacts, which have a larger influence on low  $k$  values. Especially for measurements at higher laser pulse repetition frequency, occasionally occurring very high signal peaks (compare inset B1 in Figure 6B) are the reason for the observed deviations. They are associated with the average plasma lifetime of approximately 200  $\mu$ s, which is

deduced from the length of recorded pulses. Despite the rotation of the sample, at higher repetition rates, the probability increases that a laser pulse reignites the still fading plasma from the preceding laser pulse. While this signal enhancement benefits can be exploited for example, in double-pulse LIBS experiments or in engine laser ignition,<sup>36,37</sup> it cannot be controlled reliably in the given case. To minimize these signal deviations, pulse frequency must be adjusted to plasma lifetime or averaging over a great number of signals, for example,  $k \geq 10$ , has to be done.

Nevertheless, these deviations have only little influence on the quality of fits, as the high reproducibility of correlation factors  $R^2$  demonstrates. Further, their average values are consistently above 0.975, even for low numbers of averaged signals  $k$ , indicating good fitting quality. Due to the occasionally occurring high signal intensities at 5 kHz, the relative standard deviations are slightly higher at 400–410 nm ( $RSD_{\max} \sim 2\%$  for  $k = 5$ ) than in the range 360–370 nm ( $RSD_{\max} \sim 1.5\%$  for  $k = 5$ ). Nevertheless, the results clearly show good reproducibility of the LIBS technique on lead detection with a photodiode down to a limit of five averaged signals. Leaving out the first 200 pulses is recommended for reaching a stable laser intensity, which corresponds to a continuous laser operation or suitable

start-up conditions. Finally, a minimum analysis time of 1 ms is achieved using a measurement repetition rate of 5 kHz.

Besides fitting the parameters for different numbers of averaged laser pulses, the theoretical minimum threshold for lead detection was calculated for both accessible spectral ranges. This limit of detection (LOD) conventionally is determined by.

$$\text{LOD} = \frac{3\sigma}{m},$$

where  $\sigma$  is the standard deviation in the signal of a sample with no or at least the minimum analyte content, and  $m$  is the slope of the employed calibration curve.<sup>34</sup> Considering the already determined slopes for the linear fit, and differentiation at the lowest measured lead content for the quadratic fit, LOD was determined for different numbers of averaged pulses  $k$ . The results are shown in Table 3.

Due to the spectral sensitivity of the photodiode, the calculated LOD in spectral range 1 (360-370 nm) is approximately ten times higher than in spectral region 2 (400-410 nm). Considering the standard deviations, almost comparable values of LOD are reached in range 2 for all numbers of  $k$ . The slightly smaller LOD values at low values of  $k$  are explained by the natural variations in plasma

**TABLE 3** Calculated values of the limit of detection (LOD) in both spectral ranges for different number of averaged signals  $k$

$k$	LOD in (wt%)	
	360-370 nm	400-410 nm
5	$4.8 \pm 1.36$	$0.5 \pm 0.18$
10	$5.8 \pm 1.20$	$0.6 \pm 0.17$
25	$6.6 \pm 1.02$	$0.6 \pm 0.16$
50	$6.7 \pm 0.94$	$0.6 \pm 0.15$
100	$6.8 \pm 0.89$	$0.7 \pm 0.13$

emissivity. The overall noise is reduced for measurements of adjacent plasma signals due to similar sample conditions. That means choosing a small number of averaged pulses does not significantly change the theoretical detection limit. So, the discussed reduction of evaluated signals and the consequent reduced time of measurement holds for the LOD as well.

The possibility to predict the lead content is verified by the leave-one-out-method. In this cross validation, calibration curves are constructed for all but one of the known lead contents of the samples, regarding this one as unknown. Then the lead content of the omitted sample is determined and compared with the known value. In general, the predictive ability of any quantitative model is improving at midrange concentrations.<sup>38</sup> With respect to glass-recycling determination of minor lead concentrations is requested, too. Therefore, in our work, the application of the method was limited to leaving out only the smallest theoretically predictable lead content, which corresponds to sample 2 for both spectral regions. The calculated values of lead in sample 2 for different number of averaged signals  $k$  are depicted as boxplots in Figure 7 and compared to the known lead content of  $5 \pm 0.1$  wt%. Again, each filled square is the mean and each line marks the median within each box. The box itself represents the standard deviation, while the whiskers indicate again the lowest and the highest datum, respectively, still within three times the standard deviation.

As already observed before, mean and median do not vary much over the number of averaged signals  $k$ , validating again the possibility to reduce measurement time. However, both values tend to underestimate the known lead content in both spectral ranges. Matches occur only within the standard deviation of the averaged calculated values, as indicated by the box size. Especially for smaller  $k$ , some outlier appears in both spectral ranges. Additionally, in spectral range 2 (400-410 nm), rather huge values of standard deviation arise. This can be explained by the influence of the potassium lines and the application of

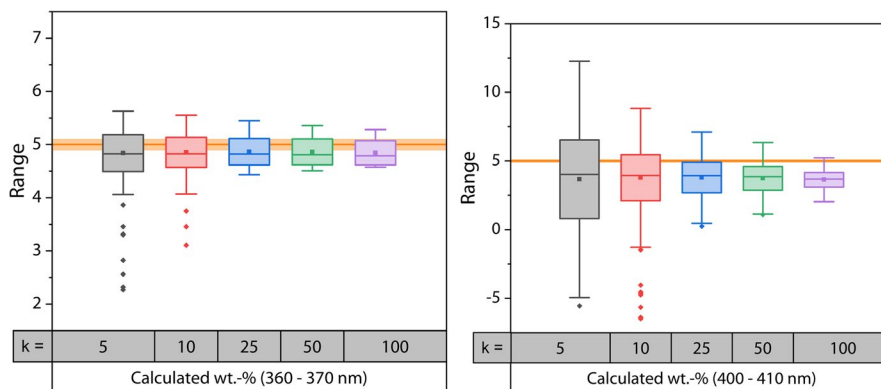


**FIGURE 7** Comparison of the known lead content of sample 2 ( $5 \pm 0.1$  wt%, orange) with the calculated lead content by the leave-one-out-method. Within each box, the filled square is the mean and the line marks the median. The box itself represents the standard deviation, while the whiskers indicate the lowest respectively highest datum still within three times the standard deviation

very simple correction factors. Nevertheless, a preferably exact determination of lead content, for example, in forensic applications, is not the goal in this work. Instead, lead detection in general and a good reproducibility are the main objectives to guarantee a high detection rate and minimize the risk of wrong or no detection. Within the standard deviation, the lowest approachable content of lead in each case is detected in both spectral ranges for almost all combinations of signals and thus can be sorted out in a later step. Merely in the second spectral range, 5% of all combinations (for  $k = 5$ ) lead to misdetection here defined by the number of signal values below 0 wt%. If necessary, this could be improved with the help of a more sophisticated approach to determine the applied correction factors for potassium or better adapted band pass filters. Further, a shift to lower values of LOD, especially in spectral range 1, can be accomplished by utilizing a photodiode with matched UV-sensitivity.

### 3.4 | Comparison with XRF

To show the potential feasibility of the developed LIBS system for sorting of lead glass, a comparison with a commercial XRF sorting machine is discussed. As already stated in the introduction, commercially available sorting machines are able to cope with material streams up to 28 tons per hour and sortable size ranges between 3 and 60 mm. Depending on the employed conveyor belt speed, typical detection times are in the range of a few milliseconds. The limit of detection also depends on belt speed, distance to the detection unit and element and is reported to be in the low percentage area. Detection efficiency is quoted 98% for particle sizes bigger than 16 mm.<sup>21,39</sup>

As shown above, the developed photodiode-LIBS setup reaches reliable detection times down to 5 ms by omitting the first 200 signals in each measurement. This was necessary due to the experimental conditions, where the laser start-up before each measurement lead to power and thus signal fluctuations. In sorting application, this delay can be compensated, for example, by powering up the laser shortly before analysis of each shard, or by continuous pulsed operations. Thus, both measurement techniques deliver comparable measurement times.

With the current setup, limits of detection of approximately 6 wt% (spectral range 1) and 0.6 wt% (spectral range 2) can be reached. Typical values of lead in recycled container glass cullet, which may rise up to 30 wt% for full lead crystal glass can thus be detected. Moreover, these detection limits are comparable to values of industrial scale XRF-systems. Nevertheless detection limits have to be further improved, for example, by a better adapted photodiode, which can be emphasized by the following rough estimation: A container glass life cycle of 40 days, from container glass creation to usage, collection of recycled glasses (10% losses) and remelting is assumed. Further, a starting value of 10 ppm lead in the raw batch, and a content of 1% of lead containing shreds

(6000 ppm) in each remelting process is estimated. In total, this leads to an accumulation of lead above 250 ppm after only six cycles or 240 days. If LOD is reduced by a factor of 10, which roughly corresponds to an average lead content of cullet of 500 ppm,<sup>9,40</sup> overall lead content will not rise over 60 ppm, if a constant share of lead-containing shreds is assumed. In the case that this share is annually increased by 20%, 250 ppm leads are reached not after approximately 10 years. Besides the detection limit, for the given application case, a reliable and reproducible detection of lead within the limits of detection plays an important role. With the present setup, only 5% of all combinations of signals in spectral range 2 lead to a wrong classification of lead-containing glass samples as lead free, while in spectral range 1 lead was detected reliably over all signal combinations. Again, comparable values to industrial scale XRF-sorting are reached.

Another benefit of the developed setup is the rather low cost of the employed hardware, which may lead to an economical use in future applications. However, for a successful implementation in a sorting machine, further aspects have to be considered, like scanning any random sequence of shards on a conveyor. Possible solutions may either be a funnel-shaped convergence of the feeding conveyer belt or, similar to established XRF-sorting machines, the utilization of multiple lasers and detectors. Further, even for the well-shaped samples employed in this work, a relatively stable focus position of the laser has to be guaranteed to get comparable signal strengths and minimize the risk of misdetection. This will become particularly important for irregular shaped shards, which occur more likely in the recycling application case. Here, the use of a convenient autofocus-system, a back-scattering measurement geometry as well as a preceding mechanical size separation can reduce the signal dependence of sample geometry. The latter already is implemented in commercially available XRF sorting machines, as X-ray-intensity also is dependent on sample geometry and thus distance to the detector by the inverse-square law. These adaptations will be subject of future studies.

Nevertheless, with comparable measurement times, accuracy, and detection limits some important parameters are fulfilled, which clearly show the feasibility of CO<sub>2</sub>-LIBS based on photodiode signal recording for lead detection in glass sorting.

## 4 | CONCLUSION

In the present study, the feasibility of CO<sub>2</sub>-LIBS as an alternative tool for the detection of lead in industrial recycling glass sorting was investigated and compared to state-of-the-art X-ray fluorescence technique. To facilitate fast detection rates, a combination of spectral filters and photodiode was employed. Glass specimens with different

amount of lead were investigated in two spectral ranges at different pulse frequencies with respect to detection limits, detection speed and accuracy. It was shown, that detection times of 5 ms can be achieved with the setup. The limits of detection were 6 wt% at range 1 (360–370 nm) and 0.6 wt% at range 2 (400–410 nm). By averaging over different numbers of recorded signals it was found, that 5% of all combinations of signals in spectral range 2 lead to a wrong classification of lead containing glass samples as lead free, while in spectral range 1 lead was detected more reliable over all signal combinations.

As comparable measurement times, accuracy of measurement, and detection limits are achieved for CO<sub>2</sub>-LIBS compared to XRF, important prerequisites are fulfilled that generally make the use of CO<sub>2</sub>-LIBS with photodiode signal recording for lead detection in glass sorting feasible.

## ACKNOWLEDGMENT

Financial support by the European Regional Development Fund (EFRE Bayern, GlasTAOO, 20-3066-03-16) is gratefully acknowledged.

## ORCID

Sebastian Lehmann  <https://orcid.org/0000-0001-7130-8502>

Andreas Rosin  <https://orcid.org/0000-0001-8835-5057>

## REFERENCES

1. EU Glass Packaging Closed Loop Recycling Steady at 74 percent; 2018 [cited 2019 Mar 4]. <https://feve.org/wp-content/uploads/2018/04/Rec-Stats-2015-Press-Release-FINAL.pdf>
2. Larsen AW, Merrild H, Christensen TH. Recycling of glass: accounting of greenhouse gases and global warming contributions. *Waste Manag Res.* 2009;27(8):754–62.
3. Beerkens R, Kers G, van Santen E. Recycling of post-consumer glass: energy savings, CO<sub>2</sub> emission reduction, effects on glass quality and glass melting. In: Drummond CH, editor. A collection of papers presented at the 71st conference on glass problems. The Ohio State University, Columbus, Ohio, October 19–20, 2010. Hoboken, NJ: Wiley; 2011. p. 167–94 (Ceramic engineering and science proceedings; vol. 32,1) [cited 2019 Mar 4]. <https://ceramics.onlinelibrary.wiley.com/doi/pdf/10.1002/9781118095348.ch16>
4. Deng W, Wright R, Boden-Hook C, Bingham PA. Melting behavior of waste glass cullet briquettes in soda-lime-silica container glass batch. *Int J Appl Glass Sci.* 2019;10(1):125–37.
5. Hynes MJ, Jonson B. Lead, glass and the environment. *Chem Soc Rev.* 1997;26(2):133.
6. Wu X, Cobbina SJ, Mao G, Xu H, Zhang Z, Yang L. A review of toxicity and mechanisms of individual and mixtures of heavy metals in the environment. *Environ Sci Pollut Res Int.* 2016;23(9):8244–59.
7. Ross CP. Heavy Metal issues - in and out of glass. In: Drummond CH, editor. A collection of papers presented at the 71st Conference on Glass Problems. The Ohio State University, Columbus, Ohio, October 19–20, 2010. Hoboken, NJ: Wiley; 2011 (Ceramic engineering and science proceedings; vol. 32,1) [cited 2019 Sep 11]. <https://ceramics.onlinelibrary.wiley.com/doi/pdf/10.1002/9781118095348.ch5>
8. Rebeniak M, Wojciechowska-Mazurek M, Mania M, Szynal T, Strzelecka A, Starska K. Exposure to lead and cadmium released from ceramics and glassware intended to come into contact with food. *Rocz Panstw Zakl Hig.* 2014;65(4):301–9.
9. Glass Technology Services LTD. Investigation Of The Significant Factors In Elemental Migration From Glass In Contact With Food; 2002 [cited 2019 Nov 19]. <https://www.glass-ts.com/projects/investigation-of-the-significant-factors-in-elemental-migration-from-glass-in-contact-with-food>
10. Gesetzüber das Inverkehrbringen, die Rücknahme und die hochwertige Verwertung von Verpackungen: Verpackungsgesetz - VerpackG; 2017 In: Bundesgesetzblatt. p. 2234–61 [cited 2019 May 21]. [https://www.bgbl.de/xaver/bgbl/start.xav?start=//%5B@attr\\_xml:id=%27%27%5d#\\_\\_bgbl\\_\\_%2F%2F\\*%5B%40attr\\_id%3D%27bgbl117s2234.pdf%27%5D\\_\\_1558428071762](https://www.bgbl.de/xaver/bgbl/start.xav?start=//%5B@attr_xml:id=%27%27%5d#__bgbl__%2F%2F*%5B%40attr_id%3D%27bgbl117s2234.pdf%27%5D__1558428071762)
11. Council Directive 84/500/EEC of 15 October 1984 on the approximation of the laws of the Member States relating to ceramic articles intended to come into contact with foodstuffs: 84/500/EEC; 1984. (vol 27) [cited 2019 Nov 19]. <https://eur-lex.europa.eu/eli/dir/1984/500/oj>
12. Position paper on food contact materials; 2019 [cited 2019 Nov 19]. <https://glassforeurope.com/food-contact-materials/>
13. Food KE.Contact Materials - Regulation (EC) 1935/2004: European Implementation Assessment: European Parliamentary Research Service; 2016 [cited 2019 Nov 19]. [http://www.europarl.europa.eu/RegData/etudes/STUD/2016/581411/EPRS\\_STU\(2016\)581411\\_EN.pdf](http://www.europarl.europa.eu/RegData/etudes/STUD/2016/581411/EPRS_STU(2016)581411_EN.pdf)
14. Dyer TD. Glass Recycling. In: Worrell E, Reuter MA, editors. Handbook of recycling: State-of-the-art for practitioners, analysts, and scientists. Amsterdam, Boston, Heidelberg, London, New York, Oxford, Paris, San Diego, San Francisco, Sydney, Tokyo: Elsevier, 2014; p. 191–209.
15. Miyoshi H, Chen D, Akai T. A novel process utilizing subcritical water to remove lead from wasted lead silicate glass. *Chem Lett.* 2004;33(8):956–7.
16. Jani Y, Hogland W. Reduction-melting extraction of trace elements from hazardous waste glass from an old glasswork's dump in the southeastern part of Sweden. *Environ Sci Pollut Res Int.* 2017;24(34):26341–9.
17. Erzat A, Zhang F-S. Evaluation of lead recovery efficiency from waste CRT funnel glass by chlorinating volatilization process. *Environ Technol.* 2014;35(21–24):2774–80.
18. Beckhoff B. Handbook of practical X-ray fluorescence analysis. Berlin Heidelberg: Springer-Verlag GmbH, 2006.
19. Trejos T, Koons R, Weis P, Becker S, Berman T, Dalpe C, et al. Forensic analysis of glass by  $\mu$ -XRF, SN-ICP-MS, LA-ICP-MS and LA-ICP-OES: evaluation of the performance of different criteria for comparing elemental composition. *J Anal At Spectrom.* 2013;28(8):1270.
20. Weiss MXRF—Applications in sensor-based-sorting using X-ray fluorescence. In: Thomé-Kozmiensky KJ, Thiel S, editors. Waste management. Nietwerder: TK Verlag Karl Thomé-Kozmiensky; 2012 (vol. 3) [cited 2017 Feb 2].
21. REDWAVE XRF-G; 2019 [cited 2019 May 20]. <http://www.redwave.com/en/recycling/glass/sensor-based/redwave-xrf-g/>
22. Lin Q-Y, Duan Y-X. Laser-induced breakdown spectroscopy: from experimental platform to field instrument. *Chin J Anal Chem.* 2017;45(9):1405–14.

23. Noll R, Fricke-Begemann C, Connemann S, Meinhardt C, Sturm V. LIBS analyses for industrial applications—an overview of developments from 2014 to 2018. *J Anal At Spectrom*. 2018;33(6):945–56.
24. Negre E, Motto-Ros V, Pelascini F, Lauper S, Denis D, Yu J. On the performance of laser-induced breakdown spectroscopy for quantitative analysis of minor and trace elements in glass. *J Anal At Spectrom*. 2015;30(2):417–25.
25. Hahn DW, Omenetto N. Laser-Induced Breakdown Spectroscopy (LIBS), part II: review of instrumental and methodological approaches to material analysis and applications to different fields. *Appl Spectrosc*. 2012;66(4):347–419. <https://www.osapublishing.org/viewmedia.cfm?uri=as-66-4-347&seq=0>
26. Cremers DA, Radziemski LJ. *Handbook of laser-induced breakdown spectroscopy*. Chichester, John Wiley & Sons, 2013.
27. Thornton B, Takahashi T, Sato T, Sakka T, Tamura A, Matsumoto A, et al. Development of a deep-sea laser-induced breakdown spectrometer for in situ multi-element chemical analysis. *Deep Sea Res Part I*. 2015;95:20–36.
28. Markiewicz-Keszycka M, Cama-Moncunill X, Casado-Gavaldà MP, Dixit Y, Cama-Moncunill R, Cullen PJ, et al. Laser-induced breakdown spectroscopy (LIBS) for food analysis: a review. *Trends Food Sci Technol*. 2017;65:80–93.
29. Lasue J, Cousin A, Meslin P-Y, Mangold N, Wiens RC, Berger G, et al. Martian eolian dust probed by ChemCam. *Geophys Res Lett*. 2018;45(20):10,968–77.
30. Noll R, Fricke-Begemann C, Brunk M, Connemann S, Meinhardt C, Scharun M, et al. Laser-induced breakdown spectroscopy expands into industrial applications. *Spectrochim Acta Part B*. 2014;93:41–51.
31. Miziolek AW. *Laser induced breakdown spectroscopy: (LIBS); Fundamentals and applications*. Cambridge: Cambridge University Press, 2008.
32. Hahn DW, Omenetto N. Laser-induced breakdown spectroscopy (LIBS), part I: review of basic diagnostics and plasma-particle interactions: still-challenging issues within the analytical plasma community. *Appl Spectrosc*. 2010;64(12):335–66.
33. Kramida A, Ralchenko Y. NIST atomic spectra database, NIST standard reference database 78. 1999.
34. El Haddad J, Canioni L, Bousquet B. Good practices in LIBS analysis: review and advices. *Spectrochim Acta Part B*. 2014;101:171–82.
35. Takahashi T, Thornton B. Quantitative methods for compensation of matrix effects and self-absorption in Laser Induced Breakdown Spectroscopy signals of solids. *Spectrochim Acta Part B*. 2017;138:31–42.
36. Babushok VI, DeLucia FC, Gottfried JL, Munson CA, Miziolek AW. Double pulse laser ablation and plasma: laser induced breakdown spectroscopy signal enhancement. *Spectrochim Acta Part B*. 2006;61(9):999–1014.
37. Lorenz S, Bärwinkel M, Stäglich R, Mühlbauer W, Brüggemann D. Pulse train ignition with passively Q-switched laser spark plugs. *Int J Engine Res*. 2015;17(1):139–50.
38. Jasik J, Heitz J, Pedarnig JD, Veis P. Vacuum ultraviolet laser-induced breakdown spectroscopy analysis of polymers. *Spectrochim Acta Part B*. 2009;64(10):1128–34.
39. Weiss M. Resource recycling in waste management with X-ray fluorescence [Diploma thesis]. Leoben: Montanuniversität Leoben, 2011.
40. Toxics in Packaging Clearinghouse. Glass Matrix Test Methods Evaluation for Toxics in Packaging; 2014 [cited 2019 Nov 19]. <https://toxicsinpackaging.org/wp-content/uploads/2014/11/GlassMatrixReport-Final-Report-Feb-2014.pdf>

**How to cite this article:** Lehmann S, Fischer M, Rosin A, Gerdes T, Krenkel W. The feasibility of CO<sub>2</sub>-laser-induced breakdown spectroscopy for fast lead determination in glass cullet. *Int J Appl Glass Sci*. 2020;11:369–379. <https://doi.org/10.1111/ijag.14653>